International Communications in Heat and Mass Transfer 116 (2020) 104683

Contents lists available at ScienceDirect

International Communications in Heat and Mass Transfer

journal homepage: www.elsevier.com/locate/ichmt

An integrated model of the thermoregulatory and respiratory systems of the human body

C. Albuquerque[a,*], J.I. Yanagihara[b]

[a] Department of Mechanical Engineering, Centro Universitário FEI, Av. Humberto de Alencar Castelo Branco, 3972, São Bernardo do Campo, SP 09850-901, Brazil
[b] Department of Mechanical Engineering, Polytechnic School, University of São Paulo, Av. Prof. Mello Moraes, 2231, São Paulo, SP 05508-030, Brazil

ARTICLE INFO

Keywords:
Bioheat transfer
Respiratory system
Thermoregulation

ABSTRACT

This work aims to develop a mathematical model for computing the distribution of temperature, O_2, and CO_2 in the human body, depending on the ambient conditions. The body is divided into segments, including layers of tissues and blood compartments, where mass and energy balances are applied. The inclusion of O_2 and CO_2 transfer mechanisms throughout all segments and tissues of the human body is one of the great novelties of this work. It also includes the exothermic metabolic reactions in the tissues, the transportation of O_2 and CO_2 by the blood, and the energy exchanged with the environment through the skin and by ventilation. The model also includes the regulation of metabolism, circulation, ventilation, and sweating, depending on the body temperature and the concentrations of O_2 and CO_2 in the blood. The lungs are represented by alveolar and blood compartments, with diffusion between them. Comparisons with experimental data from the existing literature show that the proposed model is suitable for representing transient exposure to cold and warm ambient temperatures, low concentration of O_2, and high concentrations of CO_2. In the end, some results demonstrate the effect of ambient temperature on the distribution of temperature, O_2, and CO_2 across segments, blood, and tissues. Shivering in a cold environment reduces the concentration of O_2 and increases the concentration of CO_2 in the muscles, which results in increased ventilation and blood circulation. The concentration of gases in the skin depends mainly on variations in the skin's circulation with the environment, which alters the availability of O_2 and the elimination of CO_2. Small variations were found in the concentrations of O_2 and CO_2 in the brain and lungs.

1. Introduction

The thermoregulatory and respiratory systems are related to the energy generation processes of the human body. The primary functions of the respiratory system are to transport O_2 from the ambient air to the tissues and remove CO_2 from the tissues to the environment. During the metabolic process, the tissues use O_2 and produce CO_2 and energy, which is converted into heat and work to enable the performance of activities. The primary function of the thermoregulatory system is to maintain the body temperature within ranges suitable for its operation. Several mechanisms in the human body interact with both of these systems, including blood circulation and pulmonary ventilation, which are regulated using signals of body temperature, activity level, and concentrations of O_2 and CO_2.

Most models of the respiratory system found in the literature are based on the representation of lung, blood, and tissues by compartments, where mass balances are applied [1]. Between the compartments, fluid flow or gas diffusion may occur. This concept is based on the pioneering model of Grodins et al. [2], with compartments representing the tissues and the lung. To represent the variation in ventilation and cardiac output, models usually include equations that depend on O_2 and CO_2 concentrations. Several recent models of the respiratory system have been built, including new features depending on the application. Among them, there are models to represent situations of hypoxia and hypercapnia [3–8], periodic breathing and apnea [9–11], altitude [12,13], and carbon monoxide exposure [14–17].

To represent the behavior of the thermoregulatory system, the human body is usually represented by segments with internal layers of tissue [1,18]. Blood circulates between the central region and the tissues by compartments that represent the large vessels. In tissues, temperature variation depends on conduction, blood perfusion, and metabolism, and it is determined by the Pennes eq. [19]. Depending on the application, equations are included to represent vasomotor mechanism, sweating, and shivering, which vary depending on internal and skin temperatures. The pioneering models of Wissler [20] and Stolwijk and

* Corresponding author.
E-mail addresses: cyroan@fei.edu.br (C. Albuquerque), jiy@usp.br (J.I. Yanagihara).

https://doi.org/10.1016/j.icheatmasstransfer.2020.104683

Available online 24 June 2020

Hardy [21] are the basis of the models developed to the present day. Recent models have been developed for different applications, such as for variations in environmental conditions [22–25], thermal comfort [26,27], cardiac surgery [28], asymmetric conditions [29], childrens [30], thermal transients [31], integration with detailed circulatory system [32], influence of clothes [33], elderly subjects [34], and thermoregulatory arteriovenous anastomoses [35,36].

Few authors have developed models that integrate the respiratory system with the thermoregulatory system, along with the integration of the transport of heat, O_2, and CO_2. Downey and Seagrave [37] developed a model for studying water exchange in the human body. In this work, the human body was divided into compartments representing the lungs, the central part, the muscles and the skin. The model included balances of energy and mass, gas transport equations in the blood along with temperature effects, relationships between O_2 consumption and CO_2, and heat production via metabolism, depending on physical activity. The authors included controllers for blood flow in the skin and muscle, ventilation and sweat rate. They calculated the variation of water in the body by the balance between ingested water, water lost in urine, water lost in sweat evaporation and wasted water. Model results were compared with experimental results regarding exposure to hot environments with and without water ingestion. Ji and Lui [38] developed a model of the brain with the aim of studying the advantage of hypothermia during resuscitation of the brain, which decreases O_2 consumption, against increased blood viscosity, which decreases blood flow and O_2 distribution. The decrease in O_2 consumption along with temperature is represented by the Q_{10} effect. The blood vessels were represented by several compartments arranged in series, with diffusion to the brain, and transport equations to represent the blood O_2 transport. Their results, which used sheep data, showed that the effect of decreasing blood flow is not significant. Gaohua and Kimura [39] developed a model to study breathing management during a hypothermic brain treatment. The human body was divided into several compartments, representing the places in which blood and tissues are present, with diffusion between them. The model included the cooling cover and the mechanical ventilator used in the treatment. Energy and mass balances were applied in each compartment. The Q_{10} effect and the transport equations of the gases in the blood were included. The model was validated in situations of hypoxia and hypercapnia. The authors concluded that mechanical ventilation during treatment should be controlled by the amount of cooling, so that the oxygenation of the brain remains stable.

The present work focuses on modeling the mechanisms of transport of energy, O_2, and CO_2 in the human body, including the interactions between them. The proposed model differs from others of its kind because it considers the segmented body, with the respiratory and thermoregulatory systems integrated into each member of the human body. The development of the model was based on two works carried out by the group [17,24], including features from several other models.

2. Mathematical model

2.1. Human body geometry

The human body is divided into segments, in the form of a parallelogram or a circular cross-section cylinder (Fig. 1). The segments are composed of layers of tissues with similar characteristics. The anatomical model of Ferreira and Yanagihara [24] was used for the definition of the segments and the layers, for a male subject, 67 kg in mass, 1.76 m in height, 1.8 m^2 of body surface area, and 14% body fat. Table 1 shows the limits of the tissue layers in each segment.

2.2. Circulation

The blood vessels are separated into small and large vessels. In small vessels, the temperature of the blood is considered to be the same as that of the tissues [40]. An arterial and a venous compartment are added to each segment to represent the blood that is inside the great vessels. The circulation of blood in a segment is shown in Fig. 2. In the trunk, blood circulates from the arterial to the venous compartment through pulmonary capillary compartments, while exchanging O_2 and CO_2 with a compartment that contains the gases of the alveolar space.

2.3. Large vessels

From energy balances, the temperature of the blood in the arterial compartment and in the venous compartment are obtained. They depend on the variation of the enthalpy of the blood stream and the heat transfer between the compartments:

$$V_{ar}\,\rho_{bl}\,c_{bl}\,\frac{dT_{ar}}{dt} = \dot{V}_{ar}\,\rho_{bl}\,c_{bl}\,(T_{ar}^{in} - T_{ar}) + H_{av}\,(T_{ve} - T_{ar}) \tag{1}$$

$$V_{ve}\,\rho_{bl}\,c_{bl}\,\frac{dT_{ve}}{dt} = \rho_{bl}\,c_{bl}\,(\dot{V}_{sv}\,\overline{T}_t + \dot{V}_{ve}^{in}\,T_{ve}^{in} - \dot{V}_{ve}\,T_{ve}) + H_{av}\,(T_{ar} - T_{ve}) \tag{2}$$

where: V_{ar} is the volume of the arterial compartment [m^3], from [24]; ρ_{bl} is the density of the blood, equal to 1059 kg m^{-3} [41]; c_{bl} is the specific heat capacity of the blood, equal to 3850 J kg $^{-1}$ K^{-1} [41]; T_{ar} is the temperature of the arterial compartment blood [K]; $\dot{V}_{ar}$ is the volumetric flow rate of blood through the arterial compartment [m^3 s^{-1}]; $T_{ar}{}^{in}$ is the temperature of the arterial blood coming from the previous segment or the lung [K]; H_{av} is the coefficient of heat transfer between the large vessel compartments [W K^{-1}], from [24]; V_{ve} is the volume of the venous compartment [m^3], from [24]; T_{ve} is the temperature of the venous compartment blood [K]; $\dot{V}_{sv}$ is the volumetric flow rate of blood through the segment small vessels [m^3 s^{-1}]; $\overline{T}_t$ is the average temperature of the segment tissues and small vessels blood [K]; $\dot{V}_{ve}^{in}$ is the volumetric flow rate of blood to the next segments [m^3 s^{-1}]; $T_{ve}{}^{in}$ is the average temperature of the venous blood coming from the next segments [K]; and $\dot{V}_{ve}$ is the volumetric flow rate of blood through the venous compartment [m^3 s^{-1}].

The concentration of O_2 and CO_2 in the blood of the large vessel compartments are determined by mass balances:

$$V_{ar}\,\frac{dC_{g,ar}}{dt} = \dot{V}_{ar}\,(C_{g,ar}^{in} - C_{g,ar}) \tag{3}$$

$$V_{ve}\,\frac{dC_{g,ve}}{dt} = \dot{V}_{sv}\,\overline{C}_{g,sv} + \dot{V}_{ve}^{in}\,C_{g,ve}^{in} - \dot{V}_{ve}\,C_{g,ve} \tag{4}$$

where: g is the gas O_2 or CO_2; $C_{g,\,ar}$ is the g concentration in the blood of the arterial compartment [mol m^{-3}]; $C_{g,\,ar}{}^{in}$ is the g concentration in the arterial blood coming from the previous segment or the lung [mol m^{-3}]; $C_{g,\,ve}$ is the g concentration in the blood of the venous compartment [mol m^{-3}]; $\overline{C}_{g,sv}$ is the average g concentration in the blood of the segment small vessels [mol m^{-3}]; and $C_{g,\,ve}{}^{in}$ is the g concentration in the venous blood coming from the next segments [mol m^{-3}].

2.4. Tissues and small vessels

The temperature of the tissues and the blood in the small vessels is obtained from the solution of the bioheat equation from Pennes [19]. The temperature variation depends on the heat conduction, the blood perfusion, and the metabolism:

$$\rho_t\,c_t\,\frac{\partial T_t}{\partial t} = k_t\,\nabla^2 T_t + \hat{\dot{V}}_{sv}\,\rho_{bl}\,c_{bl}\,(T_{ar} - T_t) + \hat{\dot{q}}_t \tag{5}$$

where: ρ_t is the density of the tissue [kg m^{-3}]; c_t is the specific heat capacity of the tissue [J kg $^{-1}$ K^{-1}]; T_t is the temperature of the tissue [K]; k_t is the heat conductivity of the tissue [W m^{-1} K^{-1}]; $\hat{\dot{V}}_{sv}$ is the specific volumetric flow rate of the blood through the small vessels [s^{-1}]; and $\hat{\dot{q}}_t$ is the specific heat generation of the tissues [W m^{-3}].

Table 2 shows the properties of the tissues used in the present

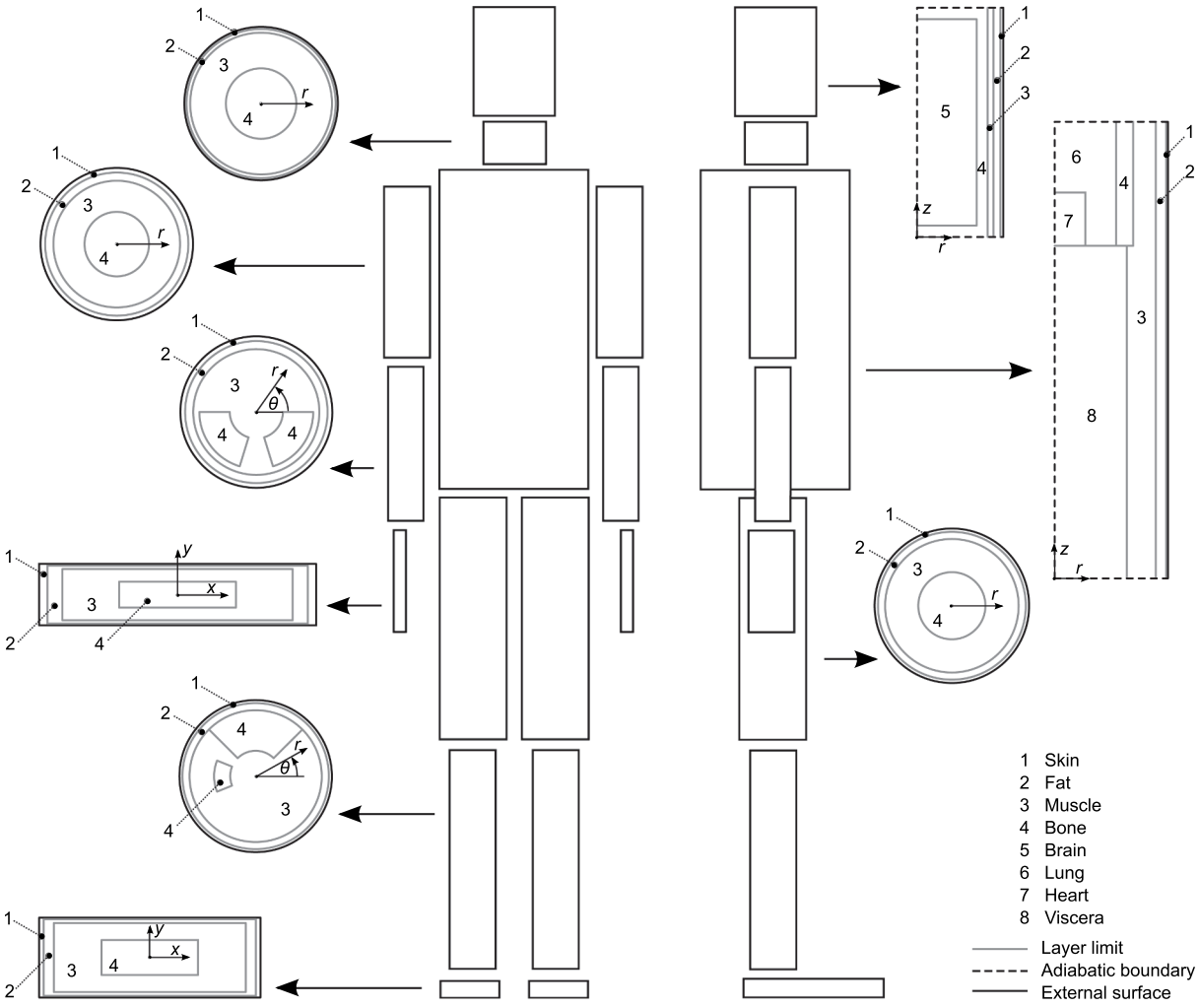

Fig. 1. Model geometry.

Table 1
Limits of the tissue layers in each segment.

Segment	Coordinate	
	r [cm] or x [cm]	θ [°], z [cm] or y [cm]
Head	5.17 6.15 6.64 7.24 7.51	1 19 20
Neck	2.68 5.40 5.71 5.82	8
Trunk	3.68 7.37 8.66 9.41 12.13 13.36 13.58	43.7 50.7 60.0
Arm	1.80 3.54 4.00 4.26	31
Forearm	1.17 2.51 2.78 3.14 3.35	180 253 287 360
Hand	3.31 9.22 3.15 7.74 9.96 10.55 10.89	0.0736 0.205 0.699 1.72 2.21 2.34 2.42
Thigh	2.68 5.33 5.90 6.15	44
Leg	1.43 3.43 3.72 4.12 4.29	45 135 158 202
Foot	0.210 0.680 2.88 7.33 9.53 10.00 10.21	0.0760 0.246 1.04 2.65 3.45 3.62 3.70

model, which were obtained from literature data.

To obtain the concentration of O_2 and CO_2 in the tissues and blood of the small vessels, a different approach is used. For each type of tissue of a segment, two compartments were included, one for the tissue, and another for the blood that is inside the small vessel of this tissue. Both compartments are considered to have the same partial pressure, as in

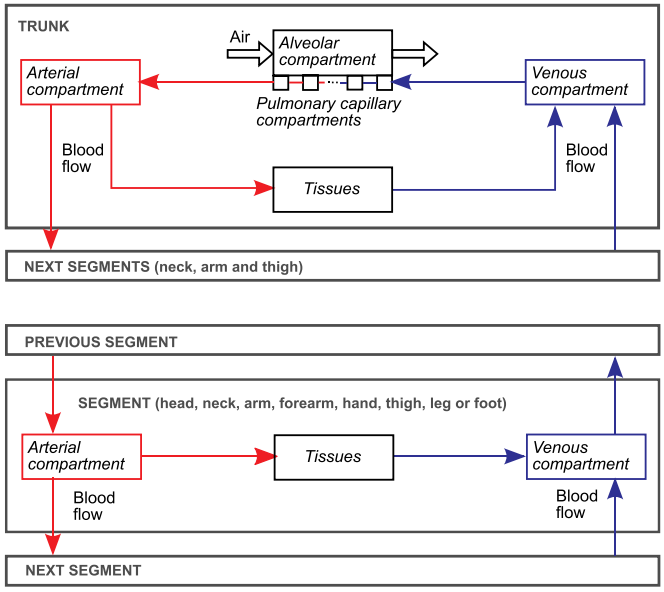

Fig. 2. Circulation inside a segment.

Table 2
Tissue parameters ([1] [24], [2] [41], [3] [42], [4]Adjusted to ensure coherence results, [5] [21], [6] [43])

Parameter	Skin	Fat	Muscle	Bone	Brain	Lung	Heart	Viscera
Tissue volume [cm^3][1]	245	528	393	860	1514	2481	298	10301
Density [kg m^{-3}][1,2]	1085	920	1085	1357	1080	560	1080	1080
Basal specific blood flow [cm^3 m^{-3} s^{-1}][1,2]	362	77	483[3]	0	9000		14400	5800[4]
Heat capacity [J kg^{-1} K^{-1}][1,2]	3680	2300	3800	1700	3850	3520	2550	3504
Heat conductivity [W m^{-1} K^{-1}][1,2]	0.47	0.21	0.51	0.75	0.49	0.28	0.47	0.49
Basal specific heat production [W m^{-3}][1,2]	368	78.2[4]	501[5]	0	9472	339	24128	3852[4]
Respiratory quotient [−][6]	0.85	0.71	0.85		1.00		0.85	0.85

Table 3
Heat transfer coefficients by convection [53], radiation [53], and evaporation [24].

Segment	Convection (h_c)	Radiation (h_r)	Evaporation (h_e)
	[W m^{-2} K^{-1}]	[W m^{-2} K^{-1}]	[W m^{-2} Pa^{-1}]
Head	3.6	4.1	0.059
Neck	3.6	4.1	0.059
Trunk	3.2	4.3	0.053
Arm	2.9	5.2	0.048
Forearm	3.7	4.9	0.061
Hand	4.1	4.1	0.068
Thigh	4.1	4.3	0.068
Leg	4.1	5.3	0.068
Foot	5.1	3.9	0.084

[17]. The partial pressure of each gas depends the on variation in concentration due to the passage of blood, and the CO_2 production or O_2 consumption by the metabolism:

$$\left(V_{sv(i)}\frac{dC_{g,sv(i)}}{dP_{g,t(i)}}+V_{t(i)}\frac{dC_{g,t(i)}}{dP_{g,t(i)}}\right)\frac{dP_{g,t(i)}}{dt}=\dot{V}_{sv(i)}\left(C_{g,ar}-C_{g,sv(i)}\right)+\dot{n}_{g,t} \quad (6)$$

where: i is the tissue type; $V_{sv(i)}$ is the volume of the small vessel compartment i [m^3] (determined as a fraction of the volume of blood in the small vessels, weighted by the specific volumetric flow rate through the small vessels); $C_{g,\,sv(i)}$ is the g concentration in the blood of the small vessel compartment i [mol m^{-3}]; $P_{g,\,t(i)}$ is the g partial pressure in the tissue and the blood of the small vessel compartment i [Pa]; $V_{t(i)}$ is the volume of the tissue compartment i [m^3] (volume of tissue subtracted by the volume of the small vessel compartment); $C_{g,\,t(i)}$ is the g concentration in the tissue of the tissue compartment i [mol m^{-3}]; $\dot{V}_{sv(i)}$ is the volumetric flow rate of blood through the small vessel compartment i [m^3 s^{-1}]; and $\dot{n}_{g,t}$ is the production of g in the tissues [mol s^{-1}].

This mass balance equation, as well as some presented in the following sections, depends on the relationship between the concentration of O_2 and CO_2 in the blood and their partial pressures. For this purpose, some relationships from the literature were used. They allow the determination of the O_2 saturation [44,45] and the CO_2 concentration [46] from the O_2 and CO_2 partial pressures, temperature, and hemoglobin concentration. This methodology is detailed in [17,47].

Relationships between concentration and partial pressure are also necessary for the tissues. In this case, the concentration of a gas is considered to be proportional to its partial pressure, with solubility coefficients for each type of tissue [48]. In muscles, relationships are also included to represent the O_2 linked to myoglobin [49].

The relationship between the heat production, O_2 consumption and CO_2 production by the tissues depends on the tissue type, and is calculated according to [50], as a function of the respiratory quotient (RQ).

To describe the energy transfer processes between the skin and the environment, typical thermal comfort methodologies have been applied, in accordance with [50], with values found in the literature for the coefficients of convection, radiation, and evaporation. The following equations show the heat transfer of the body without clothes, as in the simulations presented in this paper. Clothes could be added by including their resistances to conduction and evaporation, as well as a factor for the increase in surface area [51,52]. The heat transfer by convection and radiation is:

$$\dot{q}_c+\dot{q}_r=h_c\left(T_{sk}-T_a\right)+h_r\left(T_{cl}-\overline{T_r}\right) \quad (7)$$

where: $\dot{q}_c$ is the heat transfer by convection [W m^{-2}]; $\dot{q}_r$ is the heat transfer by radiation [W m^{-2}]; h_c is the convective heat transfer coefficient [W m^{-2} K^{-1}]; T_{sk} is the skin temperature [°C]; T_a is the air temperature [°C]; h_r is the radiative heat transfer coefficient [W m^{-2} K^{-1}]; and $\overline{T_r}$ is the mean radiant temperature [°C].

The calculation of energy transfer by evaporation is done by multiplying the maximum amount of evaporation, when the skin is saturated with water, by the fraction of wet surface (w). Analogous to convection, energy transfer by evaporation depends on the difference between the water vapor partial pressure on the skin surface ($P_{w,\,sk}$) and in the air ($\phi_a P_{w,\,a}$):

$$\dot{q}_e=w\,h_e\left(P_{w,sk}-\phi_a P_{w,a}\right) \quad (8)$$

where: $\dot{q}_e$ is the energy transfer by evaporation [W m^{-2}]; w is the fraction of wet surface [0–1]; h_e = evaporative energy transfer coefficient [W Pa^{-1}.m^{-2}]; $P_{w,\,sk}$ is water vapor partial pressure on the skin surface [Pa]; ϕ_a is the air relative humidity [0–1]; and $P_{w,\,a}$ is the air water vapor partial pressure [Pa]; The values for the heat transfer coefficients of each segment are shown in Table 3.

2.5. Respiratory apparatus

The lungs are represented by a compartment containing the gases from the alveolar space, and several compartments in series containing the blood that passes through the pulmonary capillaries. The alveolar concentration of O_2 and CO_2 depends on the conditions of the inspired air and the gas diffusion within the blood in the pulmonary capillaries:

$$V_A\frac{dP_{g,A}}{dt}=\dot{V}_A\frac{P_{bar}}{P_{bar,0}}\left(P_{g,I}-P_{g,A}\right)+\beta_g P_{bar}\sum_{k=1}^{N_{cp}}D_{g,L(k)}\left(P_{g,cp(k)}-P_{g,A}\right) \quad (9)$$

where: V_A is the volume of the alveolar compartment, equal to 2481 cm^3 [54]; $P_{g,\,A}$ is the g partial pressure in the air of the alveolar compartment [Pa]; $\dot{V}_A$ is the volumetric flow rate of air through the alveolar compartment (alveolar ventilation) [m^3 s^{-1}, STPD]; P_{bar} is the barometric pressure [Pa]; $P_{bar,\,0}$ is the barometric pressure at sea level [Pa]; $P_{g,\,I}$ is the g inspired air partial pressure [Pa]; β_g is a factor to convert from molar base to volumetric [STPD], equal to 0.0224 m^3 mol^{-1} for O_2, and 0.02226 m^3 mol^{-1} for CO_2; k is the index of the pulmonary capillary compartment [1 to 10]; N_{cp} is the amount of pulmonary capillary compartments, equal to 10; $D_{g,\,L(k)}$ is the coefficient of diffusion of g through the pulmonary membrane [mol s^{-1} Pa^{-1}], from [17], as a function of cardiac output; and $P_{g,\,cp(k)}$ is the g partial pressure in the blood of the pulmonary capillary compartment k [Pa].

The inspired air is humidified in the respiratory tract before reaching the alveolar space. Its partial pressure is determined by:

$$P_{g,I}=F_{g,I}\left(P_{bar}-P_w\right) \quad (10)$$

where: $F_{g,\,I}$ is the fraction of g in the inspired air [0 to 1]; and P_w is the water vapor pressure at the lung temperature [Pa].

The use of pulmonary capillary compartments in series makes a more accurate representation of the pulmonary diffusion, with local variation of the driving force, allowing for representation common situations such as the total O_2 saturation occurring in the first compartments. Venous blood enters the first pulmonary capillary compartment. Part of this blood (2%) ends up deviating from the lung and mixes with the blood that leaves the last pulmonary capillary to the arterial compartment. As well as the treatment made for the tissues and small vessels, a tissue compartment is added for each pulmonary capillary compartment, representing the tissues of the lungs, where metabolism occurs. The partial pressure of each gas is considered equal in blood and tissue. The partial pressure of O_2 or CO_2 in the pulmonary capillary compartment is determined by the following equation:

$$\left(V_{cp(k)}\frac{dC_{g,cp(k)}}{dP_{g,cp(k)}} + V_{t(k)}\frac{dC_{g,t(k)}}{dP_{g,cp(k)}}\right)\frac{dP_{g,cp(k)}}{dt} = \dot{V}_{cp}(C_{g,cp(k-1)} - C_{g,cp(k)}) + D_{g,L(k)}(P_{g,A} - P_{g,cp(k)}) + \dot{n}_{g,t(k)} \quad (11)$$

where: $V_{cp(k)}$ is the volume of the pulmonary capillary compartment k, equal to $140/N_{cp}$ cm^3 [55]; $C_{g,\,cp(k)}$ is the g concentration in the blood of the pulmonary capillary compartment k [mol m^{-3}]; $V_{t(k)}$ is the volume of the pulmonary tissue compartment k, equal to $161/N_{cp}$ cm^3 (estimated from the other volumes); $C_{g,\,t(k)}$ is the g concentration in the tissue of the pulmonary tissue compartment k [mol m^{-3}]; $\dot{V}_{cp}$ is the volumetric flow rate of the blood through the pulmonary capillary compartments [m^3 s^{-1}]; and $\dot{n}_{g,t(k)}$ is the production of the gas g in the pulmonary tissue compartment k [mol s^{-1}].

Energy transfer in ventilation occurs along the respiratory tract and lungs. These locations are represented by seven compartments (Fig. 3). The first compartment is in contact with the ambient air and contains gases from the mouth and pharynx. The second contains gases from the trachea. The third contains gases from the first bronchi and the end of the dead space. These first three compartments represent the path of the air during inspiration. The last three compartments (numbers 5, 6, and 7) represent these same spaces during expiration. This separation aims to simplify the ventilation's periodicity. In this way, ventilation through the compartments is continuous and always in the same direction. The fourth compartment represents the alveolar space. The gases are separated into dry air and water vapor. The compartments are in contact with tissues. Between them, there is heat transfer by convection and

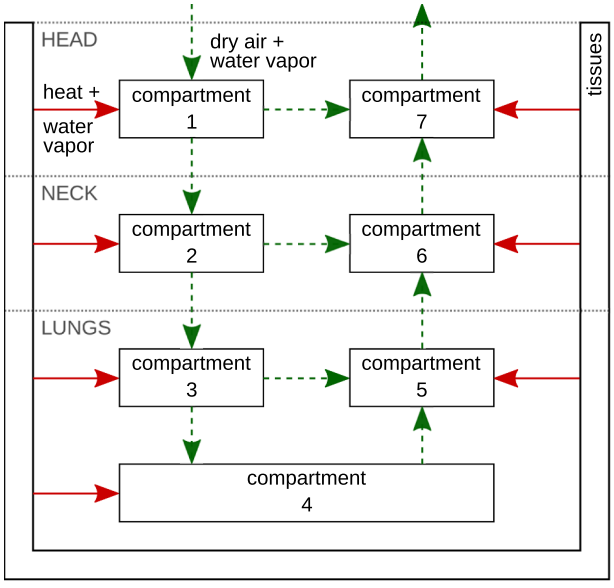

Fig. 3. Compartments of the respiratory tract.

Table 4
Characteristics of compartments used to calculate heat transfer in the respiratory tract [54,56,57].

Compartment	Volume [cm^3]	Superficial area [m^2]
1 and 7	22.0	0.00440
2 and 6	30.5	0.00679
3 and 5	103.5	0.595
4	2180	70

evaporation of water. The adequacy of these compartments with the geometry of the complete human body model is made by considering that the first and last compartments are in contact with the head muscle, the second and sixth with the neck muscle, and the third, fourth, and fifth with the lungs. The flow of gases between two compartments – or between one compartment and the ambient air – is divided into dry air and water vapor flows.

The flow of dry air between the compartments is determined based on the relationships between their volumes, noting that the flow through compartments 3, 4, and 5 is the alveolar ventilation. Their volumes and surface areas are shown in Table 4. The surface areas of the compartments (with the exception of the fourth) have been calculated from the diameters, lengths, and number of branches of the ducts. The total area for each location is divided between the two compartments that represent it.

The variation of absolute humidity in the compartments is obtained from the balances of water vapor mass. The balances consider the flow of water vapor between the compartments and the environment, and the water vapor from the evaporation process in the tissues. The variation of absolute humidity in compartment i is equal to:

$$m_{a(i)}\frac{d\omega_{(i)}}{dt} = \dot{m}^{in}_{w(i)} - \dot{m}^{out}_{w(i)} + \dot{m}^{e}_{w(i)} \quad (12)$$

where $m_{a(i)}$ is the dry air mass in compartment i [kg]; $\omega_{(i)}$ is the absolute humidity in compartment i [kg^{-1}]; $\dot{m}^{in}_{w(i)}$ is the flow of water vapor entering compartment i [kg s^{-1}]; $\dot{m}^{out}_{w(i)}$ is the flow of water vapor leaving compartment i [kg s^{-1}]; and $\dot{m}^{e}_{w(i)}$ is the flow of water vapor from evaporation in compartment i [kg s^{-1}].

The flow of water vapor generated by the evaporation process, from the tissues to the compartment, is represented by a diffusion process proportional to the difference between the absolute humidity of saturated air with the tissue temperature and the absolute humidity of the compartment:

$$\dot{m}^{e}_{w(i)} = D_{rt}A_{rt(i)}(\omega_{sat(i)} - \omega_{(i)}) \quad (13)$$

where D_{rt} is the diffusion coefficient in the respiratory tract [kg m^{-2} s^{-1}]; $A_{rt(i)}$ is the compartment superficial area [m^2]; and $\omega_{sat(i)}$ is the absolute humidity of saturated air with the tissue temperature [kg^{-1}].

The determination of the temperature variation in each compartment is obtained by applying energy balances. It includes the flow of dry air and water vapor between compartments or with the environment, the heat exchanged by convection with the tissues, and the water evaporation energy. The temperature variation in the compartment i is obtained by the following equation:

$$m_{(i)}c_{v(i)}\frac{dT_{(i)}}{dt} = \dot{H}^{in}_{(i)} - \dot{H}^{out}_{(i)} - \dot{m}^{e}_{w(i)}h_{lv(i)} + \dot{q}_{(i)} \quad (14)$$

where $m_{(i)}$ is the mass of dry air and water vapor in compartment i [kg]; $c_{v(i)}$ is the specific heat capacity at constant volume [J kg^{-1} K^{-1}]; $T_{(i)}$ is the temperature in compartment i [°C]; $\dot{H}^{in}_{(i)}$ is the enthalpy of the fluid entering the compartment i [W]; $\dot{H}^{out}_{(i)}$ is the entalphy of the fluid leaving the compartment i [W]; $h_{lv(i)}$ is the specific enthalpy vaporization with the temperature of the compartment i [J kg^{-1}]; and $\dot{q}_{(i)}$ is the

heat transfer between the compartment i and the tissues [W].

The mechanisms of heat transfer between the tissue and the compartment are grouped and represented by:

$$\dot{q}_{(i)} = U_{rt} A_{rt\,(i)} (T_{t\,(i)} - T_{(i)}) \quad (15)$$

where U_{rt} is the global heat transfer coefficient between the tissue and the compartment [W m^{-2} K^{-1}]; and $T_{t(i)}$ is the temperature of the tissue connected with the compartment i [°C].

The value of the heat transfer coefficient (U_{rt}) was considered to be equal to 10 W m^{-2} K^{-1}. This value was determined with data from [58] for different branches of the respiratory tract. The value of the diffusion coefficient (D_{rt}) is 3 $\times 10^{-6}$ kg m^{-2} s^{-1}. It was estimated aiming to obtain the total value of heat transfer in the respiratory tract from [59]. This methodology leads to total values of energy transfer through ventilation similar to those obtained with the typical procedures used in thermal comfort applications [50,60].

2.6. Metabolism

The metabolism of muscular tissues may vary due to physical activity and shivering. Moreover, all tissues include the Q_{10} effect, which represents the effect of temperature on the intensity of metabolic reactions (metabolism doubles with a 10 °C rise in temperature) [22,61]. The specific heat generation in muscle is:

$$\hat{q}_m = \hat{q}_{m,0}\, 2^{(T_m - T_{m,0})/10} + \hat{q}_{sh} + \hat{q}_{at} \quad (16)$$

where: $\hat{q}_m$ is the muscle specific heat generation [W m^{-3}]; $\hat{q}_{m,0}$ is the basal muscle specific heat generation [W m^{-3}]; T_m is the muscle temperature [°C]; $T_{m,\,0}$ is the basal muscle temperature [°C]; $\hat{q}_{sh}$ is the increase in muscle specific heat generation due to shivering [W m^{-3}]; and $\hat{q}_{at}$ is the increase in muscle specific heat generation due to physical activity [W m^{-3}].

To represent the shivering, the model of Tikuisis and Giesbrecht [62] was used, where the increase in metabolism depends on the internal temperature and the average skin temperature:

$$\dot{q}_{sh} = g_{sh\,(1)} (T_{hy}^{ref} - T_{hy}) + g_{sh\,(2)} (T_{sk}^{ref} - \overline{T}_{sk}) - g_{sh\,(3)} (T_{sk}^{ref} - \overline{T}_{sk})^2 \quad (17)$$

where: $\dot{q}_{sh}$ is the increase in muscle heat generation due to shivering [W]; $g_{sh(1)}$, $g_{sh(2)}$ and $g_{sh(3)}$ are constants, equals to 74.81 W K^{-1}, 22.61 W K^{-1}, and − 0.756 W K^{-2}; T_{hy}^{ref} is the reference temperature of the hypothalamus, equal to 34.3 °C; T_{hy} is the temperature of the hypothalamus [°C]; T_{sk}^{ref} is the reference skin temperature, equal to 34.3 °C; and $\overline{T}_{sk}$ is the average skin temperature [°C]. The average skin temperature depends on the number of sensors in each segment. It is calculated using the weighting factors from [61]. The reference temperatures were determined from the thermal neutrality conditions of the present model (without regulators acting). The maximum possible value for this increase in heat generation was set to 429 W [24].

Shivering acts with different intensity in each part of the body. To obtain the specific heat generation for each segment ($\hat{q}_{sh}$), the value obtained by the eq. 17 ($\dot{q}_{sh}$) is multiplied by the fraction at which the shivering acts on the segment, before being divided by its muscle volume. The values of these fractions and muscle volumes are shown in Table 5. The increase in specific heat generation due to physical activity is determined by the same procedure. The increase in the body's heat generation is multiplied by a fraction for each segment (Table 5), and divided by the volume of muscle.

Table 5
Muscle volumes and fractions at which shivering [61] and physical activity [63] act in each segment.

Segment	Volume of muscle [cm^3]	Shivering fraction [0–1]	Physical activity fraction [0–1]
Head	393.77	0.0339	0.0
Neck	552.36	0.0436	0.0
Trunk	12,904.32	0.9025	0.3
Arm	817.33	0.00235	0.025
Forearm	503.91	0.00145	0.015
Hand	255.26	0.0002	0.005
Thigh	2934.14	0.004	0.21
Leg	1219.19	0.00165	0.09
Foot	550.96	0.00035	0.005

2.7. Circulation

The regulation of blood flow in the small vessels acts differently depending on the type of tissue. Its input signals come from the concentrations of O_2 and CO_2 (chemical effect), temperature (thermal effect), and metabolism. The following equation shows the blood flow in the small vessels in a generalized way for all types of tissue:

$$\hat{V}_{sv} = \hat{V}_{sv,0} f_{ch} f_{th} + \hat{V}_{met} \quad (18)$$

where: $\hat{V}_{sv}$ is the specific blood flow in the small vessels [m^3 m^{-3} s^{-1}]; $\hat{V}_{sv,0}$ is the specific basal blood flow in the small vessels [m^3 m^{-3} s^{-1}]; f_{ch} is the chemical effect factor [dimensionless]; f_{th} is the thermal effect factor [dimensionless]; and $\hat{V}_{met}$ is the increase in specific blood flow due to an increase in metabolism [m^3 m^{-3} s^{-1}]. The lower limit for blood flow in the small vessels is 25% of the basal blood flow, and the upper limit is 10 times the basal blood flow [24].

To represent the influence of O_2 and CO_2 on the variation in small vessels blood flow, the model developed by Ursino et al. [3] were used. The O_2 acts on all types of tissue, while the CO_2 acts only on the brain. The effect of O_2 on circulation depends on the arterial P_{O_2}, while the effect of CO_2 depends on the arterial P_{CO_2}. These partial pressures were obtained by the volumetric average of the arterial compartments of the segments. The following equation is used to represent the O_2 effect:

$$\psi_{O_2} = c_{fc(1)} [e^{(-P_{O2,ar}/c_{fc(2)})} - e^{(-P_{O2,ar}^{ref}/c_{fc(2)})}] \quad (19)$$

where: ψ_{O_2} is the effect of the O_2 on circulation [dimensionless]; $c_{fc(1)}$ and $c_{fc(2)}$ are constants, equals to 17.0 and 1490 Pa; $P_{O_2,\,ar}$ is the arterial blood O_2 partial pressure [Pa]; and $P_{O_2,\,ar}^{ref}$ is the basal arterial blood O_2 partial pressure, equal to 12.66 kPa (95 mmHg).

To represent the effect of CO_2 on the brain, the following equation is used:

$$\psi_{CO_2} = \frac{c_{fc(3)} + c_{fc(4)}/(1 + c_{fc(5)}\, e^{c_{fc(6)} \log(P_{CO2,ar})})}{c_{fc(3)} + c_{fc(4)}/(1 + c_{fc(5)}\, e^{c_{fc(6)} \log(P_{CO2,ar}^{ref})})} - 1 \quad (20)$$

where: ψ_{CO2} is the CO_2 effect in circulation [dimensionless]; $c_{fc(3)}$, $c_{fc(4)}$, $c_{fc(5)}$ and $c_{fc(6)}$ are constants, equals to 20.9, 92.8, 10,570 and − 5.251; $P_{CO2,\,ar}$ is the arterial blood CO_2 partial pressure [Pa]; $P_{CO2,\,ar}^{ref}$ is the basal arterial blood CO_2 partial pressure, equal to 5.33 kPa (40 mmHg).

These equations show the control static response. The dynamic response of the model is obtained after including a first-order time delay, with time constants equal to 10 and 20 s for the effects of O_2 and CO_2 [3]. The chemical effect factor (f_{ch}) is calculated by adding 1 to the effect of O_2, also adding the effect of CO_2 if the tissue is the brain.

Specific muscle blood flow is mostly related with metabolism. Its increase in relation to the basal value was considered to be directly proportional to the increase in the muscle's heat generation due to physical exercise, according to the following equation:

$$\hat{V}_{met} = c_{met}\, \Delta \hat{q}_m \quad (21)$$

where: c_{met} is a constant, equal to 2.914 $\times 10^{-7}$ m^3 J^{-1}, which was obtained from interpolation of experimental data from [64]; and $\Delta \hat{q}_m$ is the variation in specific muscle's heat generation from basal conditions [W m^{-3}].

To determine the effect of temperature variation on blood flow in small vessels of the skin and muscle, some relations from Wissler [65] are used. The flow variation includes factors for the effects of internal

temperature (f_i), average skin temperature ($f_{\overline{sk}}$), local skin temperature (f_{sk}), and physical activity (f_{at}). The thermal factor (f_{th}) is found by the multiplication of these factors. In muscles, the thermal effect works only during vasoconstriction ($f_{th} \leq 1$). The physical activity factor only acts on the skin.

The internal temperature effect only acts when the temperature is higher than the reference ($f_i \geq 1$). Considering the temperature of the hypothalamus as representative of the internal temperature, this factor is calculated by the following equation:

$$f_i = 1 + c_{th(1)}\left[T_{hy} - T_{hy}^{ref} - c_{th(2)}\left(\overline{T}_{sk} - T_{sk}^{ref}\right)\right] \tag{22}$$

where: $c_{th(1)}$ is a constant equal to 4.6 °C^{-1}, obtained by analogy with the model from [66]; and $c_{th(2)}$ is a constant equal to 0.05.

The factor that represents the effect of the average skin temperature is represented by the following equation:

$$f_{\overline{sk}} = \frac{c_{th(3)} + \tanh\left[c_{th(4)}\left(\overline{T}_{sk} - c_{th(5)}\right)\right]}{c_{th(6)}} \tag{23}$$

where $c_{th(3)}$, $c_{th(4)}$, $c_{th(5)}$, and $c_{th(6)}$ are constants equal to 1.422, 0.275, 32, and 2.018, respectively.

The factor for the effect of local skin temperature is considered to vary linearly, with the slope depending on the skin temperature range:

$$f_{sk} = c_{th(7)}\,T_{sk} - c_{th(8)} \tag{24}$$

where: T_{sk} is the local skin temperature [°C]; $c_{th(7)}$ and $c_{th(8)}$ are constants, equals to 0.03857 and 0.3 if $T_{sk} \leq 35$ °C, equals to 0.56 and 18.55 if $T_{sk} > 35$ °C and $T_{sk} \leq 37$ °C, and equals to 1.4525 and 51.5725 if $T_{sk} > 37$ °C.

The physical activity factor (f_{at}) depends on the increase in heat generation due to physical activity:

$$f_{at} = 1 - c_{th(9)}\,\dot{q}_{at} \tag{25}$$

where $c_{th(9)}$ is a constant, equal to 6.455×10^{-4}.

2.8. Ventilation

The model of Longobardo [7] was adopted to represent the effect of O_2 and CO_2 on ventilation. Due to the location of the chemoreceptors in the body, the effect of the gases is separated into two parts: central and peripheral. The former is sensitive to the P_{CO_2} of the brain. The latter is sensitive to saturation of O_2 and P_{CO_2} of arterial blood. The alveolar ventilation ($\dot{V}_A$) is equal to the sum of the effect of these two parts. The constants were correct from the original model to represent the alveolar ventilation in STPD.

The central part is determined by the following equation:

$$\dot{V}_C = \begin{cases} c_{v(1)}\left(P_{CO_2,br} - P_{CO_2,br}^{ref}\right) & \text{if } P_{CO_2,br} \geq P_{CO_2,br}^{lim} \\ c_{v(1)}\left(P_{CO_2,br}^{lim} - P_{CO_2,br}^{ref}\right)\dfrac{P_{CO_2,br}}{P_{CO_2,br}^{lim}} & \text{if } P_{CO_2,br} < P_{CO_2,br}^{lim} \end{cases} \tag{26}$$

where: $\dot{V}_C$ is the central part's contribution to alveolar ventilation [L min^{-1}, STPD]; $c_{v(1)}$ is a constant equal to 0.988 L min^{-1} mmHg^{-1}; $P_{CO2,\ br}$ is the brain's CO_2 partial pressure [mmHg]; $P_{CO2,\ br}^{ref}$ is the reference brain's CO_2 partial pressure, equal to 44.35 mmHg; and $P_{CO2,\ br}^{lim}$ is the limit brain's CO_2 partial pressure, equal to 47.9 mmHg.

The peripheral part to ventilation includes the effect of O_2:

$$\dot{V}_P = \begin{cases} c_{v(2)}\left(S_{O2,ar}^{ref} - S_{O_2,ar}\right)\left(P_{CO_2,ar} - P_{CO_2,br}^{ref}\right) - c_{v(3)} & \text{if } P_{CO_2,ar} \geq P_{CO_2,ar}^{lim} \\ \left[c_{v(2)}\left(S_{O2,ar}^{ref} - S_{O_2,ar}\right)\left(P_{CO_2,ar}^{lim} - P_{CO_2,br}^{ref}\right) - c_{v(3)}\right]\dfrac{P_{CO_2,ar}}{P_{CO_2,ar}^{lim}} & \text{if } P_{CO_2,ar} < P_{CO_2,ar}^{lim} \end{cases} \tag{27}$$

where: $\dot{V}_P$ is the peripheral part's contribution to alveolar ventilation [L min^{-1}, STPD]; $c_{v(2)}$ and $c_{v(3)}$ are constants, equals to 7.79 L min^{-1} mmHg^{-1} and 0.898 L min^{-1}; $S_{O2,\ ar}^{ref}$ is the reference arterial O_2 saturation, equal to 101.72%; $S_{O2,\ ar}$ is the arterial O_2 saturation [%]; $P_{CO2,\ ar}$ is the arterial CO_2 partial pressure [mmHg]; $P_{CO2,ar}^{ref}$ is the reference arterial CO_2 partial pressure, equal to 31.123 mmHg; and $P_{CO2,ar}^{lim}$ is the limit arterial CO_2 partial pressure, equal to 38.5 mmHg.

A first-order delay (common in models of the respiratory system) was included for each part, with time constants of 60 s for the central part and 7 s for the peripheral parts [3].

2.9. Sweating

Sweating was determined in the same way as Ferreira and Yanagihara [24], to determine the wet fraction of the surface of each segment. The fraction of wet surface depends on the relationship between heat loss through evaporation and its maximum capacity:

$$w = w_{min} + (1 - w_{min})\frac{\dot{q}_e}{\dot{q}_{e,max}} \tag{28}$$

where: w is the fraction of wet surface [0–1]; w_{min} is the minimum fraction of wet surface, equal to 0.06 [50]; $\dot{q}_e$ is the heat lost by evaporation [W m^{-2}]; and $\dot{q}_{e,max}$ is the maximum capacity of the heat lost by evaporation [W m^{-2}], when the fraction of wet surface is equal to 1.

The relationship developed by Nadel et al. [67] was used to determine the heat loss by evaporation. It includes the effects of internal temperature and both average and local skin temperatures. Dependence on the local temperature value makes sweating different between segments. The following equation represents heat loss through evaporation:

$$\dot{q}_e = c_{s(1)}\left(T_{hy} - T_{hy}^{ref}\right) + c_{s(2)}\left(\overline{T}_{sk} - T_{sk}^{ref}\right)e^{\left(T_{sk} - T_{sk}^{ref}\right)/10} \tag{29}$$

where $c_{s(1)}$ and $c_{s(2)}$ are constants equal to 197 and 23 W m^{-2} °C^{-1}, respectively. The same basal references values as those described above are used.

2.10. Solution

To simulate the proposed model, an object-oriented C++ program was developed. For the heat transfer partial differential eqs. (5), the finite volume method was applied [68,69], with Cartesian or cylindrical coordinates. The discretization had 5 to 10 elements in each layer of tissue, determined via tests of the mesh to ensure negligible discretization errors.

The backward Euler method was applied to solve the ordinary and partial differential equations along time. For a new time instant, the temperatures and concentrations of O_2 and CO_2 are calculated in an implicit scheme:

$$x_t = x_{t-\Delta t} + \Delta t\, f(x_t) \tag{30}$$

where: x_t is the variable at the new time step; $x_{t-\Delta t}$ is the variable at the last time step; Δt is the time step [s]; and $f(x_t)$ is the differential equation (dx/dt). A time step of 1 s was used.

To find the values of the variables at this new instant of time (x_t), an iterative method was used. The new values of x_t are calculated using the last values of x_t, until the relative errors between all the new and old values are less than 10^{-6}. Under-relaxation was included to calculate this new value, to improve the stability of the solution. The value for a new iteration is:

$$x_{t(i+1)} = \alpha\, x_{t(i)} + (1 - \alpha)x_{t(i-1)} \tag{31}$$

where: $x_{t(i+1)}$ is the variable value that will be used as the input in the next iteration; α is the under-relaxation factor, equal to 0.1; $x_{t(i)}$ is the variable value calculated in the actual iteration; and $x_{t(i-1)}$ is the variable value calculated in the last iteration.

3. Results and discussion

The following sections present the model simulation results and compare them to experimental data found in the literature for conditions of exposure to cold and warm ambient temperatures, to low O_2 and to CO_2. Furthermore, a discussion is conducted regarding the influence of the ambient temperature on the distribution of temperature, O_2, and CO_2 over the entire body.

3.1. Exposure to a cold environment

Raven et al. [70,71] carried out cold exposure experiments with 11 subjects. The subjects were dressed only in athletic shorts. First, they stayed resting in a supine position, with air temperature of 28 ± 1 °C and relative humidity of 45 ± 2%. After some time, the subjects were moved to a neighboring chamber at 5 ± 1 °C and 70 ± 2% relative humidity. Measurements were taken every 10 min. The heat production was estimated from the respiratory gases and flow. Skin temperature was measured in several places, in addition to the internal temperature (rectal). The graphs in Fig. 4 compare the model's simulation (lines) with the experimental data (points) with the standard deviation between the subjects (error bars), for the internal temperature, the skin temperature at some positions, and the heat generation. In the simulation, the subject was nude with a resting activity (40 W m^{-2}).

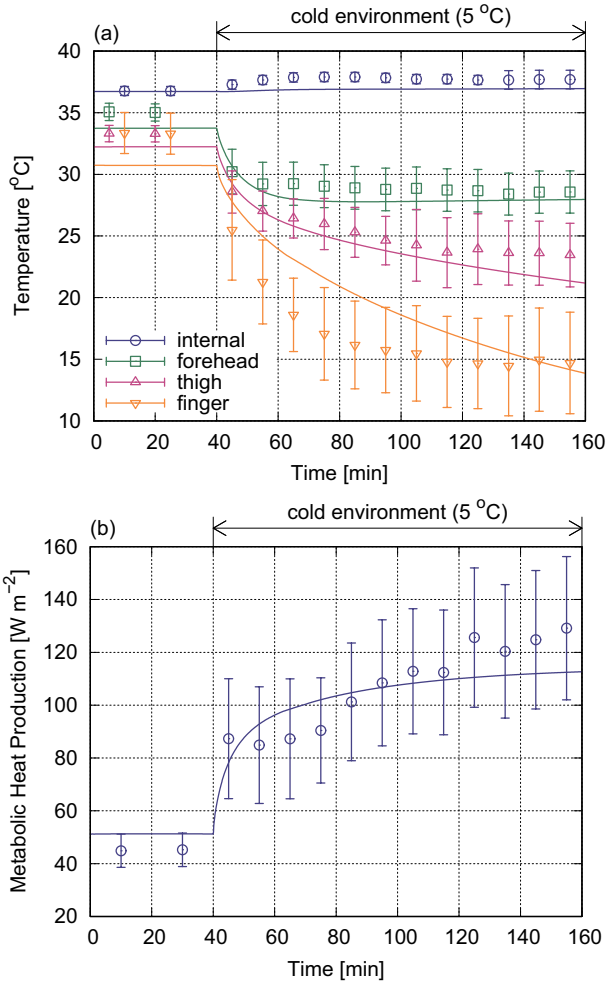

Fig. 4. Comparison of the internal temperature and some skin temperatures (a) and the metabolic heat generation (b) from the present model (lines) along with the experimental data from [70,71] (points).

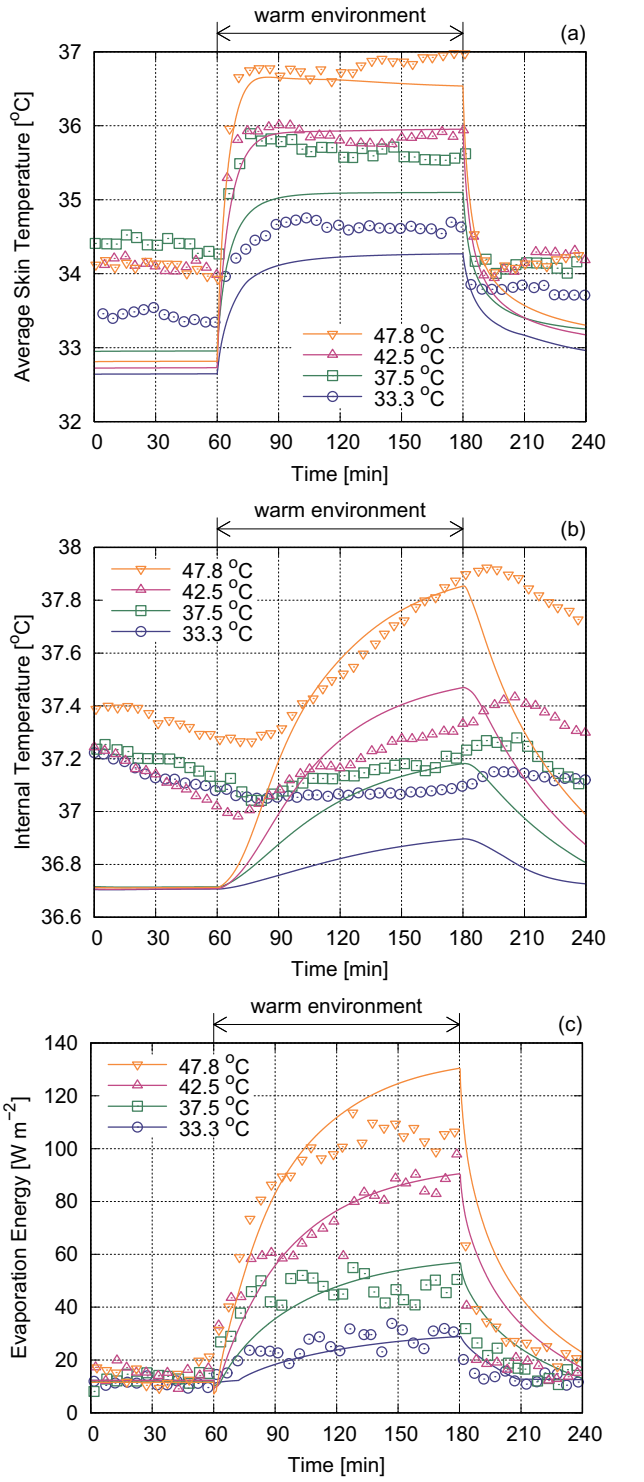

Fig. 5. Comparison of the internal temperature (a), the average skin temperature (b) and the heat lost by evaporation through the skin (b) from the present model (lines) with the experimental data from [72] (points).

The internal temperature exhibited a small increase during the cold exposure. This increase is mostly due to the effects of shivering and the vasoconstriction regulation mechanisms. The skin temperatures decrease during the cold exposure, because of the proximity to the ambient environment. The model was able to simulate the behavior of the temperatures, as well as the increase of the metabolic heat production.

3.2. Exposure to a warm environment

Stolwijk and Hardy [72] performed experiments with three subjects to study the response of the human body during exposure to a warm ambient temperature. Two chambers with controlled temperature and air humidity were used. One chamber was at 28 °C, while the other was kept at warm ambient conditions. The subjects were connected to thermocouples and then remained quiet for two hours at a neutral room temperature. After the measurements began, subjects remained for one hour in the neutral chamber, then for two hours in the warm chamber, and then returned to the neutral environment for another hour. The temperature of the neutral chamber was about 28 °C with humidity of 40%. The tests were carried out with four different temperatures of the warm chamber. Each subject engaged in the test twice for each warm temperature. The internal (tympanic and esophagus) temperature was measured, as well as the skin temperature in 10 different locations, in order to estimate an average value. The metabolism was calculated from measurements of respiratory O_2 and CO_2. The energy lost via evaporation through sweating was determined by continuously measuring the body mass variation.

The graphs in Fig. 5 present comparisons of the experimental results from [72] with the results from simulations of the model. For the simulations, the same air temperature and humidity of the experiments were used, with the body nude with a resting activity (44 W m^{-2}). The behavior of the simulations was similar to that of the experimental data for average skin temperature, internal (esophagus) temperature, and evaporation energy. All values exhibited a larger variation for higher ambient temperatures. A discrepancy was observed in terms of average skin temperature between simulation and experimental data; nevertheless, the variation of the skin temperature is very small.

3.3. Exposure to low amounts of O_2

Reynolds and Milhorn Jr. [73] carried out experiments in which 10 subjects were exposed to fractions of 9, 8, and 7% of O_2. For the measurements, a circuit was used where the air breathed by the subject was collected. Ventilation, respiratory rate, tidal volume, and alveolar P_{O2} and P_{CO2} were measured continuously, then grouped in averages every two minutes. Exposure to low O_2 fractions (in nitrogen) lasted 10 min. Subjects remained in a comfortable reclining chair during the experiment.

Fig. 6 presents comparisons of the model simulation results with the experimental data for alveolar P_{O_2} and P_{CO_2} and minute ventilation. In the simulation, a neutral environment (operating temperature of 30 °C and relative humidity of 50%) was assumed, at sea level, with the subject nude and quiet (metabolism of 44 W m^{-2}). The behavior of the alveolar P_{O_2} observed in the simulation was similar to that observed in the experiment during the exposure. In recovery after hypoxia, the alveolar P_{O_2} from simulation returns to the initial value faster than is the case for the experimental one. The shapes of the simulated and experimental alveolar P_{CO_2} are similar for all levels of hypoxia; however, the simulation values are lower than the experimental values at all times. The drop in alveolar P_{CO_2} during hypoxia occurs mainly due to the ventilation increase, which is a body response to increase the amount of inspired O_2. As a consequence, the body increases its ability to eliminate CO_2. Moreover, the simulation results for the ventilation were very similar to the experimental results.

3.4. Exposure to CO_2

Reynolds et al. [74] conducted experiments with ten subjects to analyze the alveolar P_{O2}, the alveolar P_{CO2}, and the ventilation behaviors during hypercapnia. The subjects breathed a mixture of air with 3, 5, 6 and 7% of CO_2 for 25 min. The experiment was performed with the same experimental apparatus and the same subjects as the experiment described above [73]. The experimental methodology was also the same.

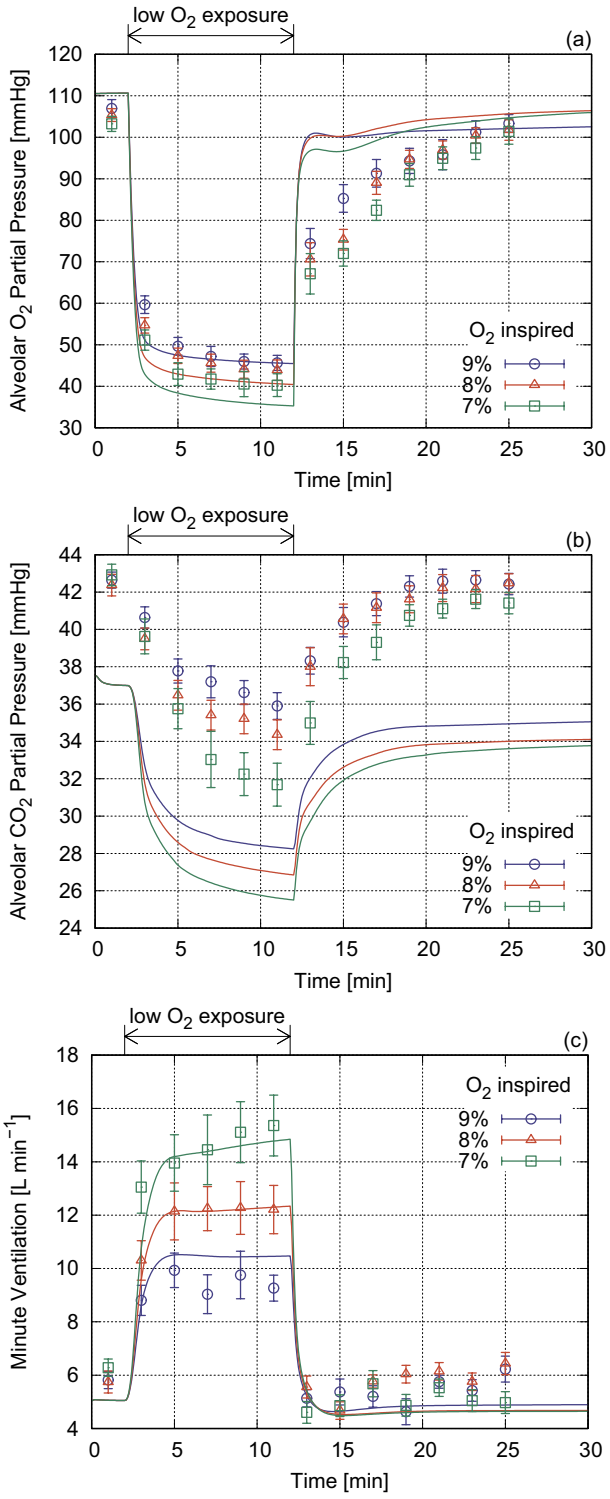

Fig. 6. Comparison of the alveolar P_{O_2} (a), alveolar P_{CO_2} (b) and the ventilation (c) from the present model (lines) with the experimental data from [73] (points).

Fig. 7 presents a comparison of the model simulation results with the experimental results. For the simulation, the conditions were an operative temperature of 30 °C, relative humidity of 50%, nude, at sea level, with the activity of a sitting and quiet person (60 W m^{-2}). The alveolar P_{O_2} exhibited a significant increase during the exposure, mostly

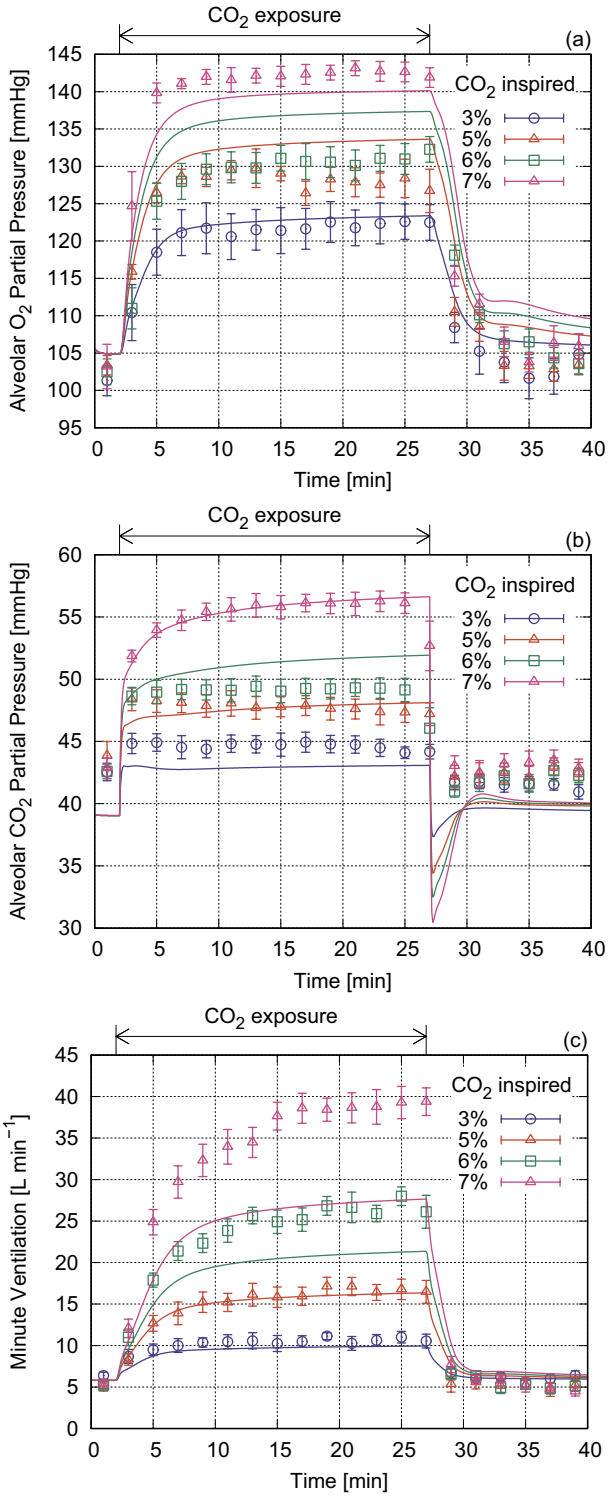

Fig. 7. Comparison of the alveolar P_{O_2} (a), alveolar P_{CO_2} (b), and the ventilation (c) from the present model (lines) with the experimental data from [74] (points).

due to the increase in ventilation to eliminate the CO_2, which causes more O_2 to be captured by the lung.

The results of the simulation for the alveolar P_{CO_2} were close to the experimental results during hypercapnia. In the recovery phase, the simulation results exhibited a sub-signal. This sub-signal occurs because the ventilation of the simulation demonstrated a slower drop than the alveolar P_{CO_2}, meaning that the lung retains a high ability to eliminate

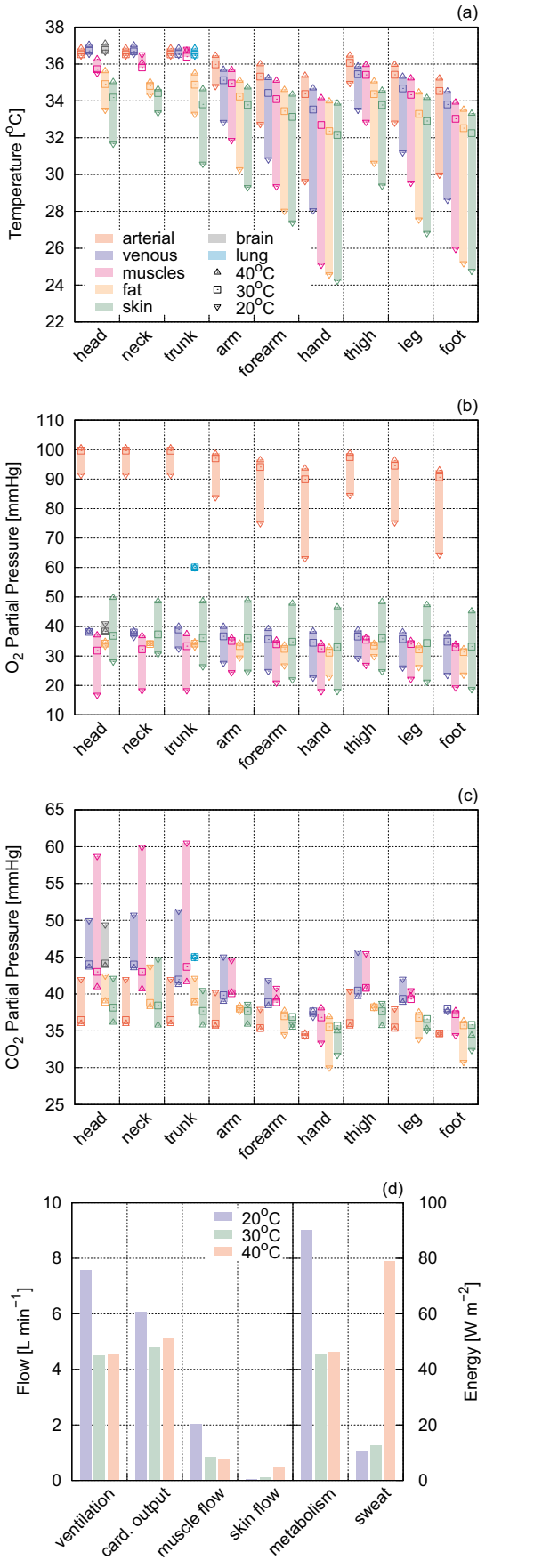

(caption on next page)

Fig. 8. Distribution of (a) temperature, (b) P_{O_2}, (c) P_{CO_2}, and (d) regulatory mechanisms for operative temperatures of 20 °C (▽), 30 °C (□), and 40 °C (Δ), with average values for the tissues and blood of all body segments. The legends for (b) and (c) are the same as (a).

CO_2 for a longer time. Although they did not appear at the experimental points on the graph, their authors argued that post-hypercapnia subsigns existed for exposures at 5, 6, and 7% of CO_2, when results are observed continuously rather than with mean values.

3.5. Air temperature effect on temperature, O_2 and CO_2 distribution

The results of this section (Fig. 8) are intended to show the changes in the human body, under a steady state, for three different operating temperatures: 20, 30 and, 40 °C. The first results, as shown in Fig. 8a, b, and c, present the average values for temperature, P_{O2}, and P_{CO2}, respectively, in the blood and tissues of all the segments. The blood and tissues of each segment are grouped. For an operative temperature of 20 °C, the average values are represented by upside-down triangles, for 30 °C by squares, and for 40 °C by regular triangles. A filled line between the minimum and maximum value for each tissue is included to clearly show its variation with the ambient temperature. In addition to these, the results show the behavior of the regulatory mechanisms under these conditions (Fig. 8d). The relative humidity was considered to be 40%, and the body was considered to be resting (45.6 W m^{-2}), nude, and at sea level.

The arterial blood exhibits a small variation because it is mostly influenced by trunk temperature. Moreover, the venous blood exhibits a more significant variation because it is formed by blood returning from the tissues. The arterial and venous blood temperatures in the trunk, neck, and head are practically the same under all ambient conditions, because of the large blood flow close to the core of the body. The brain and lung temperatures are also almost the same. The temperature variation is larger the more extreme the segment is. These results show the body's ability to maintain its most vital parts under stable thermal conditions.

When the ambient temperature is equal to 20 °C, the decrease in the temperature of the tissues causes an increase in shivering. This ends up increasing the metabolic activity in the muscles, resulting in a greater demand for O_2 and an increase in the production of CO_2. This performance is evidenced by the decrease of P_{O2} as well the increase of P_{CO2} in the muscles of the trunk, neck, and head, which are the body parts most affected by shivering. Similar variations are found in light activities, such as the intramuscular P_{O2} and P_{CO2} of 11.6 mmHg and 50.4 mmHg, respectively, found by [75] in handgrip exercises. To increase the availability of O_2 and the elimination of CO_2, the body works to increase the blood flow to the muscles and ventilation. Increased ventilation on exposure to cold was observed by [76] in studies of immersion in water at different temperatures. In the cold environment, skin vasoconstriction decreases the availability of O_2 that comes from blood, and the P_{O2} of the skin ends up decreasing. The elimination of CO_2 by the blood also decreases, resulting in an increase in the skin's P_{CO2}. As the increase in blood flow to the muscles is greater than the decrease in the blood flow to the skin, the cardiac output ends up increasing. The P_{O2} and P_{CO2} of the most vital organs, such as the brain and lungs, exhibit small variations with room temperature.

With the environmental temperature at 40 °C, the body increases the sweat and skin blood flow, to intensify the energy transfer with the environment. The increase in energy transfer associated with the evaporation of sweat needs to balance the heat transfer by convection and radiation from the environment to the body, since the temperature of the environment is higher than the temperature of the skin. P_{O_2} and P_{CO_2} have little variation in relation to the 30 °C environment. The most significant variation occurs in the skin, where vasodilation increases the availability of O_2 and elimination of CO_2 from the blood, resulting in increased P_{O_2} and decreased P_{CO_2}. The increased blood flow to the skin leads to increased cardiac output.

The response of the model had a behavior similar to the experimental results of Wener and Reents [77], obtained with six subjects in the same environmental conditions as the simulations, with measurements in different places of the body. The skin temperature was measured at points that are representative of the model's segments (except the neck). The average values of these points were 27.0, 33.7, and 36.5 °C for ambient temperatures of 20, 30, and 40 °C, respectively The average values achieved by the model were 27.9, 33.3, and 35.4 °C. For blood flow, the mean experimental values (trunk and forearm) were 172, 439, and 1661 $m^3\ cm^{-1}\ s^{-1}$, while the model had values of 247, 451, and 2249 $m^3\ cm^{-1}\ s^{-1}$. For the energy exchanged by evaporation in the skin, the average experimental results (head, trunk, arm, hand, leg, and foot) were 7.9, 15.4, and 76.9 W^{-2} for the three ambient temperatures. The model reached the values of 10.4, 12.7, and 81.6 W^{-2}.

4. Conclusion

This work presents the development of an integrated model of the human body thermoregulatory and respiratory systems. The model allows the determination of the distribuiton of the temperature, O_2 and CO_2 in blood and tissues. Its behavior is influenced by the ambient conditions and the physical activity level.

Comparisons with literature experimental data under transient state reveal that the model is suitable for representing the effect of exposures to different ambient conditions. The results show either an increase in muscle metabolism due to the shivering in a cold environment or an increase in energy lost through evaporation in a warm environment. Other results show the increase in ventilation to satisfy the tissue requirement for O_2 when its concentration in the inspired air is low, or to increase CO_2 elimination when its concentration in the air is high. Moreover, the results show the temperature, O_2, and CO_2 distribution for different air temperatures. The body exhibits small temperature variation in the central segments, and more significant variations in the more extreme segments. Finally, the amount of O_2 and CO_2 exhibits larger variations in a cold ambient temperature, mostly due to the shivering. It is worth noting that the latter results would only be possible with an integrated model.

Declaration of Competing Interest

The authors declare that they have no known competing financial interests or personal relationships that could have appeared to influence the work reported in this paper.

Acknowledgements

The authors are grateful to Fundação de Amparo à Pesquisa do Estado de São Paulo (FAPESP) for the financial support (grant number 2007/01161–7). The second author would like to acknowledge CNPq (National Council for Scientific and Technological Development - Brazil) for the research grant 309214/2017–3.

References

[1] J.I. Yanagihara, M.S. Ferreira, C. Albuquerque, Modeling of heat and mass transfer in human thermal and respiratory systems and its application to engineering and medical sciences, Proceedings of the 16th International Heat Transfer Conference, Beijing, 2018, https://doi.org/10.1615/ihtc16.kn.000016.
[2] F.S. Grodins, J.S. Gray, K.R. Schroeder, A.L. Norins, R.W. Jones, Respiratory responses to CO_2 inhalation. A theoretical study of a nonlinear biological regulator, J. Appl. Physiol. 7 (3) (1954) 283–308, https://doi.org/10.1152/jappl.1954.7.3.283.
[3] M. Ursino, E. Magosso, G. Avanzolini, An integrated model of the human ventilatory control system: the response to hypercapnia, Clin. Physiol. 21 (4) (2001) 447–464, https://doi.org/10.1046/j.1365-2281.2001.00349.x.
[4] M. Ursino, E. Magosso, G. Avanzolini, An integrated model of the human

ventilatory control system: the response to hypoxia, Clin. Physiol. 21 (4) (2001) 465–477, https://doi.org/10.1046/j.1365-2281.2001.00350.x.
[5] P.J. Liang, D.A. Bascom, P.A. Robbins, Extended models of the ventilatory response to sustained isocapnic hypoxia in humans, J. Appl. Physiol. 82 (2) (1997) 667–677, https://doi.org/10.1152/jappl.1997.82.2.667.
[6] H. Zhou, G.M. Saidel, M.E. Cabrera, Multi-organ system model of O_2 and CO_2 transport during isocapnic and poikilocapnic hypoxia, Respir. Physiol. Neurobiol. 156 (3) (2007) 320–330, https://doi.org/10.1016/j.resp.2006.11.002.
[7] G. Longobardo, C.J. Evangelisti, N.S. Cherniack, Effects of neural drives on breathing in the awake state in humans, Respir. Physiol. 129 (3) (2002) 317–333, https://doi.org/10.1016/s0034-5687(01)00325-5.
[8] Z.L. Topor, M. Pawlicki, J.E. Remmers, A computational model of the human respiratory control system: responses to hypoxia and hypercapnia, Ann. Biomed. Eng. 32 (11) (2004) 1530–1545, https://doi.org/10.1114/b:abme.0000049037.65204.4c.
[9] J.J. Batzel, H.T. Tran, Modeling instability in the control system for human respiration: applications to infant non-rem sleep, Appl. Math. Comput. 110 (1) (2000) 1–52, https://doi.org/10.1016/s0096-3003(99)00112-5.
[10] S.M. Yamashiro, Non-linear dynamics of human periodic breathing and implications for sleep apnea therapy, Med. Biol. Eng. Comput. 45 (4) (2007) 345–356, https://doi.org/10.1007/s11517-006-0153-y.
[11] K. Lu, J.W.J. Clark, F.H. Ghorbel, D.L. Ware, J.B. Zwischenberger, A. Bidani, Whole-body gas exchange in human predicted by a cardiopulmonary model, Cardiovasc. Eng. 3 (1) (2002) 1–19, https://doi.org/10.1023/A:1024795417999.
[12] M.B. Wolf, R.P. Garner, A mathematical model of human respiration at altitude, Ann. Biomed. Eng. 35 (11) (2007) 2003–2022, https://doi.org/10.1007/s10439-007-9361-3.
[13] A. Qiu, J. Bai, Multiple modeling in the study of interaction of hemodynamics and gas exchange, Comput. Biol. Med. 31 (1) (2001) 59–72, https://doi.org/10.1016/s0010-4825(00)00023-8.
[14] M. Sharan, S. Selvakumar, A mathematical model for the simultaneous transport of gases to compute blood carboxyhaemoglobin build-up due to CO exposures: application to the end-expired breath technique, Environ. Pollut. 105 (2) (1999) 231–242, https://doi.org/10.1016/S0269-7491(98)00215-2.
[15] E. Bruce, M. Bruce, A multicompartment model of carboxyhemoglobin and carboxymyoglobin responses to inhalation of carbon monoxide, J. Appl. Physiol. 95 (3) (2003) 1235–1247, https://doi.org/10.1152/japplphysiol.00217.2003.
[16] J.H. Stuhmiller, L.M. Stuhmiller, A mathematical model of ventilation response to inhaled carbon monoxide, J. Appl. Physiol. 98 (6) (2005) 2033–2044, https://doi.org/10.1152/japplphysiol.00034.2005.
[17] C. Albuquerque-Neto, J.I. Yanagihara, F. Turri, A carbon monoxide transport model of the human respiratory system applied to urban atmosphere exposure analysis, J. Braz. Soc. Mech. Sci. Eng. 30 (2008) 253–260, https://doi.org/10.1590/s1678-58782008000300011.
[18] M. Fu, W. Weng, W. Chen, N. Luo, Review on modeling heat transfer and thermoregulatory responses in human body, J. Therm. Biol. 62 (2016) 189–200, https://doi.org/10.1016/j.jtherbio.2016.06.018.
[19] H.H. Pennes, Analysis of tissue and arterial blood temperatures in the resting human forearm, J. Appl. Physiol. 1 (2) (1948) 93–122, https://doi.org/10.1152/jappl.1948.1.2.93.
[20] E.H. Wissler, Steady-state temperature distribution in man, J. Appl. Physiol. 16 (4) (1961) 734–740, https://doi.org/10.1152/jappl.1961.16.4.734.
[21] J.A.J. Stolwijk, J.D. Hardy, Temperature regulation in man – a theoretical study, Arch. Eur. J. Physiol. 291 (2) (1966) 129–162, https://doi.org/10.1007/bf00412787.
[22] D. Fiala, K.J. Lomas, M. Stohrer, A computer model of human thermoregulation for a wide range of environmental conditions: the passive system, J. Appl. Physiol. 87 (5) (1999) 1957–1972, https://doi.org/10.1152/jappl.1999.87.5.1957.
[23] D. Fiala, K.J. Lomas, M. Stohrer, Computer prediction of human thermoregulatory and temperature responses to a wide range of environmental conditions, Int. J. Biometeorol. 45 (3) (2001) 143–159, https://doi.org/10.1007/s004840100099.
[24] M.S. Ferreira, J.Y. Yanagihara, A transient three-dimensional heat transfer model of the human body, Int. Commun. Heat Mass. 36 (7) (2009) 718–724, https://doi.org/10.1016/j.icheatmasstransfer.2009.03.010.
[25] W.G. Weng, X.F. Han, M. Fu, An extended multi-segmented human bioheat model for high temperature environments, Int. J. Heat Mass Transf. 75 (2014) 504–513, https://doi.org/10.1016/j.ijheatmasstransfer.2014.03.091.
[26] C. Huizenga, H. Zhang, E. Arens, A model of human physiology and comfort for assessing complex thermal environments, Build. Environ. 36 (6) (2001) 691–699, https://doi.org/10.1016/s0360-1323(00)00061-5.
[27] L. Yi, L. Fengzhi, L. Yingxi, L. Zhongxuan, An integrated model for simulating interactive thermal processes in human–clothing system, J. Therm. Biol. 29 (7–8) (2004) 567–575, https://doi.org/10.1016/j.jtherbio.2004.08.071.
[28] N.M.W. Severens, W.D. van Marken Lichtenbelt, A.J.H. Frijns, A.A. Van Steenhoven, B.A.J.M. de Mol, D.I. Sessler, A model to predict patient temperature during cardiac surgery, Phys. Med. Biol. 52 (17) (2007) 5131–5145, https://doi.org/10.1088/0031-9155/52/17/002.
[29] M. Al-Othmani, N. Ghaddar, K. Ghali, A multi-segmented human bioheat model for transient and asymmetric radiative environments, Int. J. Heat Mass Transf. 51 (2008) 5522–5533, https://doi.org/10.1016/j.ijheatmasstransfer.2008.04.017.
[30] B.A. Ying, Y.L. Kwok, Y. Li, C.Y. Yeung, F.Z. Li, S. Li, Mathematical modeling of thermal physiological responses of clothed infants, J. Therm. Biol. 29 (7–8) (2004) 559–565, https://doi.org/10.1016/j.jtherbio.2004.08.027.
[31] D. Lai, Q. Chen, A two-dimensional model for calculating heat transfer in the human body in a transient and non-uniform thermal environment, Energy and Buildings 118 (2016) 114–122, https://doi.org/10.1016/j.enbuild.2016.02.051.
[32] M. Salloum, N. Ghaddar, K. Ghali, A new transient bioheat model of the human body and its integration to clothing models, Int. J. Therm. Sci. 46 (4) (2007) 371–384, https://doi.org/10.1016/j.ijthermalsci.2006.06.017.
[33] M. Fu, T. Yu, H. Zhang, E. Arens, W. Weng, H. Yuan, A model of heat and moisture transfer through clothing integrated with the UC Berkeley comfort model, Build. Environ. 80 (2014) 96–104, https://doi.org/10.1016/j.buildenv.2014.05.028.
[34] M. Rida, N. Ghaddar, K. Ghali, J. Hoballah, Elderly bioheat modeling: changes in physiology, thermoregulation, and blood flow circulation, Int. J. Biometeorol. 58 (9) (2014) 1825–1843, https://doi.org/10.1007/s00484-013-0785-1.
[35] W. Karaki, N. Ghaddar, K. Ghali, K. Kuklane, I. Holmér, L. Vanggaard, Human thermal response with improved AVA modeling of the digits, Int. J. Therm. Sci. 67 (2013) 41–52, https://doi.org/10.1016/j.ijthermalsci.2012.12.010.
[36] M. Rida, W. Karaki, N. Ghaddar, K. Ghali, J. Hoballah, A new mathematical model to simulate AVA cold-induced vasodilation reaction to local cooling, Int. J. Biometeorol. 58 (9) (2014) 1905–1918, https://doi.org/10.1007/s00484-014-0792-x.
[37] D. Downey, R.C. Seagrave, Mathematical modeling of the human body during water replacement and dehydration: body water changes, Ann. Biomed. Eng. 28 (3) (2000) 278–290, https://doi.org/10.1114/1.267.
[38] Y. Ji, J. Liu, Numerical studies on the effect of lowering temperature on the oxygen transport during brain hypothermia resuscitation, Comput. Biol. Med. 32 (6) (2002) 495–514, https://doi.org/10.1016/s0010-4825(02)00030-6.
[39] L. Gaohua, H. Kimura, A mathematical model of respiratory and biothermal dynamics in brain hypothermia treatment, IEEE Trans. Biomed. Eng. 55 (4) (2008) 1266–1278, https://doi.org/10.1109/tbme.2007.912400.
[40] M.M. Chen, K.R. Holmes, Microvascular contributions in tissue heat transfer, Ann. N. Y. Acad. Sci. 335 (1980) 137–150, https://doi.org/10.1111/j.1749-6632.1980.tb50742.x.
[41] J. Werner, M. Buse, Temperature profiles with respect to inhomogeneity and geometry of the human body, J. Appl. Physiol. 65 (3) (1988) 1110–1118, https://doi.org/10.1152/jappl.1988.65.3.1110.
[42] R.F. Mottram, The oxygen consumption of human skeletal muscle in vivo, J. Physiol. 128 (2) (1955) 268–276, https://doi.org/10.1113/jphysiol.1955.sp005305.
[43] J.R. Brobeck, Energy exchange, in: V.B. Mountcastle (Ed.), Medical Physiology, 13th edition, 2 C.V. Mosby Company, St. Louis, 1974, pp. 1237–1252 Ch. 53.
[44] L.J. Thomas, Algorithms for selected blood acid-base and blood gas calculations, J. Appl. Physiol. 33 (1) (1972) 154–158, https://doi.org/10.1152/jappl.1972.33.1.154.
[45] J.W. Severinghaus, Blood gas calculator, J. Appl. Physiol. 21 (3) (1966) 1108–1116.
[46] A.R. Douglas, N.L. Jones, J.W. Reed, Calculation of the whole blood CO_2 content, J. Appl. Physiol. 65 (1) (1988) 473–477, https://doi.org/10.1152/jappl.1988.65.1.473.
[47] F. Turri, J.I. Yanagihara, Computer-assisted numerical analysis for oxygen and carbon dioxide mass transfer in blood oxygenators, Artif. Organs 35 (6) (2011) 579–592, https://doi.org/10.1111/j.1525-1594.2010.01150.x.
[48] L.E. Farhi, H. Rahn, Dynamics of changes in carbon dioxide stores, Anesthesiology 21 (1960) 604–614, https://doi.org/10.1097/00000542-196011000-00004.
[49] K.A. Schenkman, D.R. Marble, D.H. Burns, E.O. Feigl, Myoglobin oxygen dissociation by multiwavelength spectroscopy, J. Appl. Physiol. 82 (1) (1997) 86–92, https://doi.org/10.1152/jappl.1997.82.1.86.
[50] ASHRAE, American Society of Heating, Refrigerating and air-Conditioning Engineers. Thermal comfort, Handbook, Fundamentals, Atlanta, 2009 (Ch. 9).
[51] E.A. McCullough, B.W. Jones, J. Huck, A comprehensive data base for estimating clothing insulation, ASHRAE Trans. 91 (2) (1985) 795–802.
[52] E.A. McCullough, B.W. Jones, T. Tamura, A data base for determining the evaporative resistance of clothing, ASHRAE Trans. 95 (2) (1989) 316–328.
[53] R.J. de Dear, E. Arens, Z. Hui, M. Oguro, Convective and radiative heat transfer coefficients for individual human body segments, Int. J. Biometeorol. 40 (3) (1997) 141–156, https://doi.org/10.1007/s004840050035.
[54] C.J. Lambertsen, Physical and mechanical aspects of respiration, in: V.B. Mountcastle (Ed.), Medical Physiology, 13th edition, 2 C.V. Mosby Company, St. Louis, 1974, pp. 1361–1371 Ch. 58.
[55] C.J. Lambertsen, The atmosphere and gas exchanges with the lungs and blood, in: V.B. Mountcastle (Ed.), Medical Physiology, 13th edition, 2 C.V. Mosby Company, St. Louis, 1974, pp. 1372–1398 Ch. 59.
[56] D.E. Olson, G.A. Dart, G.F. Filley, Pressure drop and fluid flow regime of air inspired into the human lung, J. Appl. Physiol. 28 (4) (1970) 482–494, https://doi.org/10.1152/jappl.1970.28.4.482.
[57] W.S. Fowler, Lung function studies. II. The respiratory dead space, Am. J. Phys. 154 (3) (1948) 405–416, https://doi.org/10.1152/ajplegacy.1948.154.3.405.
[58] I.M. Kandjov, Heat and water rate transfer processes in the human respiratory tract at various altitudes, J. Theor. Biol. 208 (3) (2001) 287–293, https://doi.org/10.1006/jtbi.2000.2217.
[59] R. Hanson, Respiratory heat loss at increased core temperature, J. Appl. Physiol. 37 (1974) 103–107, https://doi.org/10.1152/jappl.1974.37.1.103.
[60] P.O. Fanger, Thermal Comfort Analysis and Application in Environmental Engineering, McGraw-Hill, New York, 1970.
[61] R.G. Gordon, R.B. Roemer, S.M. Horvath, A mathematical model of the human temperature regulatory system – transient cold exposure response, IEEE Trans. Biomed. Eng. (1976) 434–444, https://doi.org/10.1109/tbme.1976.324601.
[62] P. Tikuisis, G.G. Giesbrecht, Prediction of shivering heat production from core and mean skin temperatures, Eur. J. Appl. Physiol. Occup. Physiol. 79 (3) (1999) 221–229, https://doi.org/10.1007/s004210050499.
[63] J.A.J. Stolwijk, A mathematical model of physiological temperature regulation in man, Contractor Report CR-1855, Nasa, Washington, 1971.

[64] A.N. Damato, J.G. Galante, W.M. Smith, Hemodynamic response to treadmill exercise in normal subjects, J. Appl. Physiol. 21 (3) (1966) 959–966, https://doi.org/10.1152/jappl.1966.21.3.959.
[65] E.H. Wissler, A quantitative assessment of skin blood flow in humans, Eur. J. Appl. Physiol. 104 (2) (2008) 145–157, https://doi.org/10.1007/s00421-008-0697-7.
[66] M.V. Savage, G.L. Brengelmann, Control of skin blood flow in the neutral zone of human body temperature regulation, J. Appl. Physiol. 80 (4) (1996) 1249–1257, https://doi.org/10.1152/jappl.1996.80.4.1249.
[67] E.R. Nadel, R.W. Bullard, J.A. Stolwijk, Importance of skin temperature in the regulation of sweating, J. Appl. Physiol. 31 (1) (1971) 80–87, https://doi.org/10.1152/jappl.1971.31.1.80.
[68] S.V. Patankar, Numerical Heat Transfer and Fluid Flow, Hemisphere, New York, (1980).
[69] C.R. Maliska, Transferência de calor e mecânica dos fluidos computacional, 2nd edition, LTC, Rio de Janeiro, 2004.
[70] P.R. Raven, S.M. Horvath, Variability of physiological parameters of unacclimatized males during a two-hour cold stress of 5°C, Int. J. Biometeorol. 14 (3) (1970) 309–320, https://doi.org/10.1007/BF01742075.
[71] P.B. Raven, I. Niki, T.E. Dahms, S.M. Horvath, Compensatory cardiovascular responses during an environmental cold stress, 5 °C, J. Appl. Physiol. 29 (4) (1970) 417–421, https://doi.org/10.1152/jappl.1970.29.4.417.
[72] J.A.J. Stolwijk, J.D. Hardy, Partitional calorimetric studies of responses of man to thermal transients, J. Appl. Physiol. 21 (3) (1966) 967–977, https://doi.org/10.1152/jappl.1966.21.3.967.
[73] W.J. Reynolds, H.T. Milhorn Jr., Transient ventilatory response to hypoxia with and without controlled alveolar PCO2, J. Appl. Physiol. 35 (2) (1973) 187, https://doi.org/10.1152/jappl.1973.35.2.187.
[74] W.J. Reynolds, H.T. Milhorn Jr., G.H. Holloman Jr., Transient ventilatory response to graded hypercapnia in man, J. Appl. Physiol. 33 (1) (1972) 47–54, https://doi.org/10.1152/jappl.1972.33.1.47.
[75] B.R. Soller, R.D. Hagan, M. Shear, J.M. Walz, M. Landry, D. Anunciacion, A. Orquiola, S.O. Heard, Comparison of intramuscular and venous blood ph, pco2 and po2 during rhythmic handgrip exercise, Physiol. Meas. 28 (6) (2007) 639–649, https://doi.org/10.1088/0967-3334/28/6/003.
[76] I.B. Mekjavic, J. Bligh, The increased oxygen uptake upon immersion, Eur. J. Appl. Physiol. Occup. Physiol. 58 (5) (1989) 556–562, https://doi.org/10.1007/bf02330712.
[77] J. Werner, T. Reents, A contribution to the topography of temperature regulation in man, Eur. J. Appl. Physiol. Occup. Physiol. 45 (1) (1980) 87–94, https://doi.org/10.1007/BF00421205.